Communication

Comparison of Ceria-Supported Catalysts for Attaining NO - NO2 Equilibrium at Industrial Nitric Acid Plant Conditions

Jithin Gopakumar * , Albert Miró i Rovira , Bjørn Christian Enger , David Waller , Magnus Rønning

Posted Date: 10 October 2023

doi: 10.20944/preprints202310.0537.v1

Keywords: the ostwald process; nitric acid; fertilizer; nitric oxide; ruthenium; ceria; manganese; catalysis

Article

Comparison of Ceria-Supported Catalysts for Attaining NO - NO_2 Equilibrium at Industrial Nitric Acid Plant Conditions

Jithin Gopakumar [1], Albert Miro i Rovira [1], Bjørn Christian Enger [2], David Waller [3] and Magnus Rønning [1,*]

[1] Norwegian University of Science and Technology (NTNU), Department of Chemical Engineering, Sem Sælands vei 4, NO-7491 Trondheim, Norway
[2] SINTEF Industry, Kinetic, and Catalysis group, P.O. Box 4760 Torgarden, NO-7465 Trondheim, Norway
[3] YARA Technology Center, Herøya Forskningspark, Bygg 92, Hydrovegen 67, NO-3936 Porsgrunn, Norway
* Correspondence: magnus.ronning@ntnu.no

Abstract: Nitric acid is a key component in the production of nitrate fertilisers and is industrially produced using the Ostwald process. The Ostwald process can be further intensified by oxidising nitric oxide to nitrogen dioxide using heterogeneous catalysts. We have explored various monometallic and bimetallic catalysts for NO to NO_2 oxidation and found ruthenium supported on ceria, containing 10 wt.% manganese to be a promising catalyst for oxidising NO to NO_2 at low temperatures at industrially relevant conditions. For a feed comprising 10% NO, 6% O_2, 15% H_2O and rest Ar, and 8% NO, 2% NO_2 5% O_2, 15% H_2O and rest Ar, the ruthenium-manganese catalysts attained NO-NO_2 equilibrium below 400°C. For the 5wt.% ruthenium and 10 wt.% manganese on ceria catalyst, an apparent activation energy of 39.4 kJ/mol and 85.4 kJ/mol were observed in the absence and presence of NO_2, respectively. These findings demonstrate the potential of supported bimetallic ruthenium-manganese catalysts for efficient oxidation of NO to NO_2 at low temperatures which can lead to significant process intensification of nitric acid plants.

Keywords: the ostwald process; nitric acid; fertilizer; nitric oxide; ruthenium; ceria; manganese; catalysis

1. Introduction

Industrial nitric acid (HNO_3) production utilises the Ostwald process, where ammonia is mainly oxidised by air over a Pt-Rh gauze catalyst into NO and H_2O (Equation 1), followed by homogeneous gas phase oxidation of NO to NO_2 (Equation 2) and further absorption of NO_2 by water to produce nitric acid (Equation 3).

$$4\ NH_3 + 5\ O_2 \rightarrow 4\ NO + 6\ H_2O \quad \Delta H_{r298} = -907\ kJ/mol \tag{1}$$

$$2\ NO + O_2 \rightarrow 2\ NO_2 \qquad \Delta H_{r298} = -113.8\ kJ/mol \tag{2}$$

$$3\ NO_2 + H_2O \rightarrow 2\ HNO_3 + NO \quad \Delta H_{r298} = -37\ kJ/mol \tag{3}$$

The Ostwald process is a mature, extensively studied and highly optimised process for commercial nitric acid production. A typical gas composition after the ammonia combustor (Equation 1) contains 10% of NO, along with 6% O_2 and 15% H_2O at 800°C [1–3]. The gas further travels through heat exchangers with short residence times to attain a temperature range of 350-400°C. From this point onwards to the NO_2 absorption column, the NO_2 concentration in the gas stream increases due to the gas phase conversion of NO. Nitric oxide (NO) is a free radical with an unpaired electron and its oxidation can also be assumed to take place in two steps as follows [1]:

$$2NO \rightleftharpoons (NO)_2 \tag{4}$$

Preprints (www.preprints.org) | NOT PEER-REVIEWED | Posted: 10 October 2023 doi:10.20944/preprints202310.0537.v1

$$(NO)_2 + O_2 \rightleftharpoons 2NO_2 \tag{5}$$

According to Honti [1], the first dimerization reaction of NO is instantaneous with an equilibrium constant ($K_{NO_{Dimer}}$) that increases with temperature like any other exothermic reaction. If the overall rate of the NO oxidation reaction is **r**, then it depends on the rate of reaction of Eq. 5 and $K_{NO_{Dimer}}$ as follows:

$$\mathbf{r} = \frac{r'}{K_{NO_{Dimer}}}, \text{ where r' corresponds to the rate of reaction of Eq. 5} \tag{6}$$

Hence, as $K_{NO_{Dimer}}$ increases with temperature, the overall rate of the NO oxidation reaction **r** is decreasing, giving rise to an inverse Arrhenius behaviour. Homogeneous NO to NO_2 conversion (%) is calculated as follows:

$$NO_{\text{Conversion}} = \frac{\text{Concentration of } NO_2 \text{ in the outlet}}{\text{Concentration of } NO \text{ in the inlet}} \cdot 100 \tag{7}$$

Figure 1 presents NO to NO_2 equilibrium conversion (%) variation with temperature and pressure. That is, NO oxidation to NO_2 follows an inverse Arrhenius behaviour, but is proportional to pressure which is in line with Le Chatelier's principle.

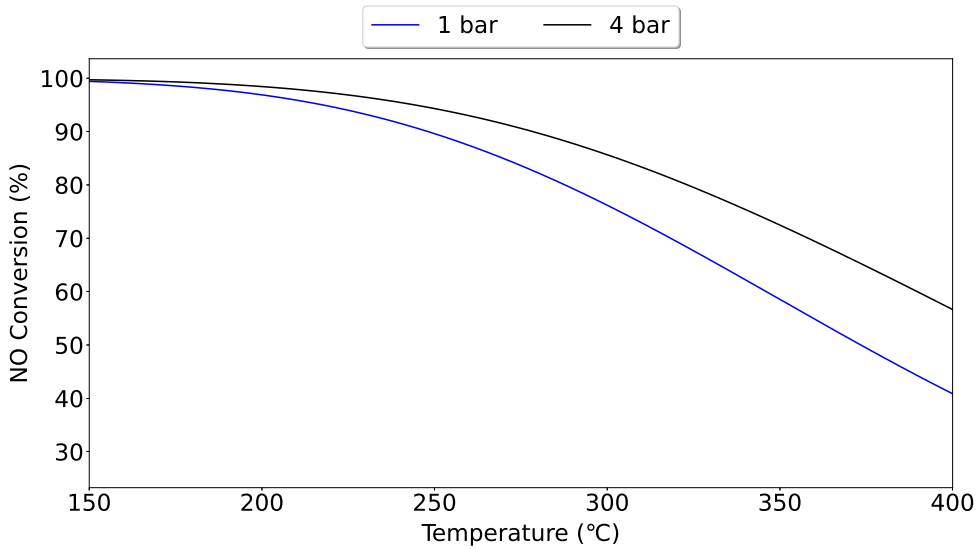

Figure 1. Homogeneous equilibrium conversion of NO to NO_2 as a function of temperature at 1 and 4 barg pressures.

Heterogeneously catalysing this bulky homogeneous gas phase oxidation of NO to NO_2 has several advantages: (1) it decreases capital expenditure (CAPEX) of new nitric acid plants, (2) thus reducing industrial footprint, and (3) significant heat recovery [4]. Grande et al.[4] evaluated the kinetics of catalytic oxidation of NO to NO_2 using a Pt/alumina catalyst at 4-5 bar pressure and found that with a stable heterogeneous catalyst that can oxidise NO to NO_2 in the range of 250-350°C, the process can be intensified by 10% in terms of energy consumed. A catalyst for NO oxidation faces two main challenges, (i) gas-phase conversion of NO to NO_2 (presented in Figure 1) and (ii) presence of strong oxidisers in the feed (NO, O_2, NO_2, HNO_2 and HNO_3). A direct result of the gas-phase conversion of NO to NO_2 is that the oxygen available for catalytic reaction becomes limited in the feed. There have been numerous studies on the oxygen storage capacities of ceria (CeO_2) and ceria-supported catalysts which enhance the activity for CO and hydrocarbon oxidation of three-way converters[5–7]. Cerium being one of the most versatile rare earth elements does not really fall into the "critical rare earth" category and has been a popular catalyst and support material since 1994 [8]. In literature, several base metal oxides such as Co oxides, Mn oxides and various perovskites have been investigated for NO oxidation at low concentrations of NO [9–13]. More than base metals, noble

 doi:10.20944/preprints202310.0537.v1

metals and particularly Pt have been studied for their NO oxidation capacity at low concentrations of NO[14–18]. Apart from the earlier publications from our group at high NO concentrations (with and without water in the feed) [12,19–21] and Grande et al.[4], only a few other early patents talk about catalytic oxidation of NO to NO_2 at conditions relevant to industrial nitric acid production [22–24]. Unlike base metals, noble metals can resist oxidation in moist air and from certain acids [25]. However, the cost of noble metals is 10-50 times higher than base metals [25,26] and almost all of the platinum group metals (PGM) are at supply risk globally [27]. Hence, designing a suitable catalyst for NO oxidation at industrial nitric acid conditions should account for not just catalytic activity but also cost, availability and global supply. However, insufficient data exist regarding the catalytic NO to NO_2 oxidation activity of various metals under industrially relevant conditions.

In this work we report the low-temperature activity of a series of ceria (CeO_2) based catalysts to attain NO-NO_2 equilibrium at industrial nitric acid production conditions. This research can assist in the optimisation and better design of a catalyst to oxidise NO at high concentrations and also serve as a starting point for catalytic activity-related research on NO oxidation at industrial nitric acid production conditions. We mainly compare transition metals, two post-transition metals and three rare earth metals. Except for osmium, all other noble metals are tested for their NO oxidation activity for comparison.

2. Materials and Methods

2.1. Catalyst Preparation

All catalysts were loaded with 5wt.% of active metal (M) on ceria (Solvay Actalys HSA10, 53-90μm) using *incipient wetness* impregnation. A calculated amount of metal precursor was first dissolved in de-ionised water and stirred at 40°C for 1hr before impregnating the precursor solution onto the support. As-prepared catalysts were dried in an oven at 120°C for 15hrs followed by calcination in air (50 Ncm^3/min) for 6hrs at 500°C. The calcined catalysts were crushed and sieved to 53-90μm sieve fraction for activity testing. For preparing Ru-Mn bimetallic catalysts, after the Ru_{CeO_2} was prepared, it was further tested for a new incipient wetness point. A calculated amount of $Mn(NO_3)_2.4H_2O$ was first dissolved in de-ionised water and dry impregnated onto the Ru_{CeO_2} catalyst, followed by drying at 120°C for 15hrs and calcination in air (50 Ncm^3/min) for 6hrs at 500°C. The details of the metal precursors and commercial suppliers are given in Table 1. The monometallic catalysts are designated M_{CeO_2} and bimetallic catalysts as M_{X_y,CeO_2}, where M corresponds to 5wt.% loaded active metal, X and y present promoter metal and its loading respectively.

2.2. Characterization

N_2 adsorption was used to measure the specific surface area of the ceria support and catalyst samples. The samples were degassed at 200°C for 12 hours in a VacPrep 061 Degasser before transferring to a Micromeritics TriStar II 3020 Analyser. Specific surface areas were calculated using the BET method at liquid nitrogen temperature (-196°C).

Ex-situ X-ray diffractograms for the support and catalyst samples were obtained using a Bruker D8 Advance X-ray Diffractometer (D8 Davinci) at 40kV and 40mA, using the wavelength of Cu K_α radiation (1.54060Å). The diffractograms were recorded in the 2θ range of 5-75° with a 0.1° slit opening.

The total metal dispersion was calculated by performing chemisorption measurements using a Micromeritics ASAP 2010S unit at 30-50°C for all fresh catalyst samples. A sample of known weight (≈80-100mg) was loaded into a U-shaped quartz reactor and the bed temperature was controlled using a thermocouple. Before chemisorption, the sample was dried at 120°C for 1hr. The isotherm was measured in the pressure range of 150-500mmHg. The chemisorption probe species and conditions were different for the different monometallic catalysts. However, the chemisorption programme for bimetallic catalysts and the Ru_{CeO_2} catalyst were the same assuming CO chemisorbing only on

Preprints (www.preprints.org) | NOT PEER-REVIEWED | Posted: 10 October 2023 doi:10.20944/preprints202310.0537.v1

ruthenium metal. Table 2 details probe gas and metal to adsorbed species ratio used for chemisorption with respect to the different catalysts.

Table 1. Designations of all ceria-based catalysts and impregnated metal precursor details.

Catalyst Name	Metal Precursor	Commercial Supplier
Cr_{CeO_2}	$Cr(NO_3)_3.9H_2O$	Sigma Aldrich
Mn_{CeO_2}	$Mn(NO_3)_2.4H_2O$	Sigma Aldrich
Fe_{CeO_2}	$FeCl_3$	Sigma Aldrich
Co_{CeO_2}	$Co(NO_3)_2.6H_2O$	Sigma Aldrich
Ni_{CeO_2}	$Ni(NO_3)_2.6H_2O$	Sigma Aldrich
Y_{CeO_2}	$Y(NO_3)_3.6H_2O$	Sigma Aldrich
Zr_{CeO_2}	$ZrO(NO_3)_2.xH_2O$	Sigma Aldrich
Nb_{CeO_2}	$NbCl_5$	Sigma Aldrich
Ru_{CeO_2}	$RuCl_3.xH_2O$	Sigma Aldrich
Ru_{Mn_5,CeO_2}	$RuCl_3.xH_2O$,$Mn(NO_3)_2.4H_2O$	Sigma Aldrich
Ru_{Mn_{10},CeO_2}	$RuCl_3.xH_2O$,$Mn(NO_3)_2.4H_2O$	Sigma Aldrich
Ru_{Mn_{15},CeO_2}	$RuCl_3.xH_2O$,$Mn(NO_3)_2.4H_2O$	Sigma Aldrich
Ru_{Mn_{20},CeO_2}	$RuCl_3.xH_2O$,$Mn(NO_3)_2.4H_2O$	Sigma Aldrich
Rh_{CeO_2}	$RhCl_3$	Sigma Aldrich
Pd_{CeO_2}	$PdCl_2$	Sigma Aldrich
Ag_{CeO_2}	$AgNO_3$	Alfa Aesar
Sn_{CeO_2}	$SnCl_4$	Sigma Aldrich
Re_{CeO_2}	$ReCl_3$	Sigma Aldrich
Ir_{CeO_2}	$IrCl_3$	Merck
Pt_{CeO_2}	$(Pt(NO_3)_4)_{aq}$	Alfa Aesar
Au_{CeO_2}	$(HAuCl_4)_{aq}$	Sigma Aldrich
Pb_{CeO_2}	$PbCl_2$	Sigma Aldrich
Gd_{CeO_2}	$Gd(NO_3)_3.6H_2O$	Alfa Aesar
Er_{CeO_2}	$Cl_3Er.6H_2O$	Sigma Aldrich

2.3. Activity Testing

Catalyst performances were evaluated as a function of temperature (150-400°C) and NO to NO_2 conversion in two different feeds; Feed (i) 10% NO, 6% O_2, 15% H_2O and rest Ar and Feed (ii) 8% NO, 2% NO_2, 5% O_2, 15% H_2O and rest Ar, with a space velocity of 24,000 $Ncm^3/g_{gcat}h$ in a tubular reactor of 9.7mm inner diameter. Conversion of NO to NO_2 (%) is calculated as:

$$NO_{\text{Conversion}} = x_{NO} = \lambda \cdot \frac{[NO_2]_{outlet}}{[NO]_{inlet}} \cdot 100 \tag{8}$$

where $[NO]_{inlet}$ and $[NO_2]_{outlet}$ are inlet and outlet concentration of NO and NO_2 of the reactor. λ = 0.99, accounts for the volume changes that arise from the reaction [28].

Further details of the experimental set-up presented in Figure 2 are given in our previous publications [12,19–21]. A dedicated set of mass flow controllers from Bronkhorst was used to feed the reactant gases. To feed 15% of water, a controlled evaporator mixer (CEM) from Bronkhorst was used. All gas lines before and after the reactor were preheated to 200°C, to ensure no cold spots for water condensation. All reactant gases (40%NO/Ar, 40%O_2/Ar, 100%H_2 and 100%Ar) were obtained from Linde-Gass AS. NO_2 during activity testing was produced *in-situ*, and for calibration of the *in-situ* produced NO_2 a new 10%NO_2/Ar (Total pressure: 8.85 bar) gas bottle was purchased from Linde-Gass AS.

Boyle's law is commonly used to predict the volume of gas when the pressure changes and vice versa. The law only holds true for gases that follow the ideal gas law. However, since NO_2 is highly reactive and unstable, it does not obey the ideal-gas law and also does not follow Boyle's law. Nitric oxide (NO) oxidation to nitrogen dioxide (NO_2) can be summarised as [1]:

$$2NO + O_2 \longrightarrow 2NO_2 \rightleftharpoons N_2O_4 \qquad \Delta H_{r_{298}} = -113.8\text{kJ/mol} \tag{9}$$

Preprints (www.preprints.org) | NOT PEER-REVIEWED | Posted: 10 October 2023 doi:10.20944/preprints202310.0537.v1

Changing pressure and temperature has an effect on the equilibrium between NO_2 and N_2O_4 (Equation 9). As temperature increases, the proportion of NO_2 increases and as pressure increases the proportion of N_2O_4 increases. This property of NO_2 makes it challenging to pressurise and produce pressurised gas bottles with higher concentrations. As the concentration of NO_2 in the gas bottle increases, the total pressure obtained on the gas bottle for supply decreases. As a result, the purchased $10\%NO_2/Ar$ bottle has only 8.85 bar pressure for process operations. To overcome this challenge for catalyst activity testing, higher concentrations of NO_2 in feed(ii) were produced *in-situ* using a method that utilises homogeneous oxidation capacity of nitric oxide when mixed with oxygen at room temperature and ambient pressure (described briefly in Section S1).

The product stream was analysed using an infrared gas analyser (MKS MultiGas 2030-HS FTIR Gas Analyser, 5.11m path length) that gives direct composition for NO, NO_2, N_2O, H_2O, NH_3, HNO_2 and HNO_3 using pre-calibrated data obtained from MKS. To monitor inert Ar, N_2 and O_2, a mass spectrometer (Pfeiffer Vacuum ThermoStar GSD 301 T3 Benchtop Mass Spectrometer) was used to ensure the absence of excess O_2 while producing NO_2 *in-situ*. The apparent activation energy was calculated far from equilibrium in both feed compositions (i) and (ii), at WHSV= 24,000 $Ncm^3/g_{gcat}h$ at 1bar in the temperature range of 340-350 °C using Arrhenius plot. Prior to activity testing, the catalyst samples were activated in $5\%H_2/Ar$ as a function of temperature (30-500°C) with a heating rate of 5°C/min in a space velocity of 24,000 $Ncm^3/g_{gcat}h$ and subsequently cooled down to 150°C inside the reactor.

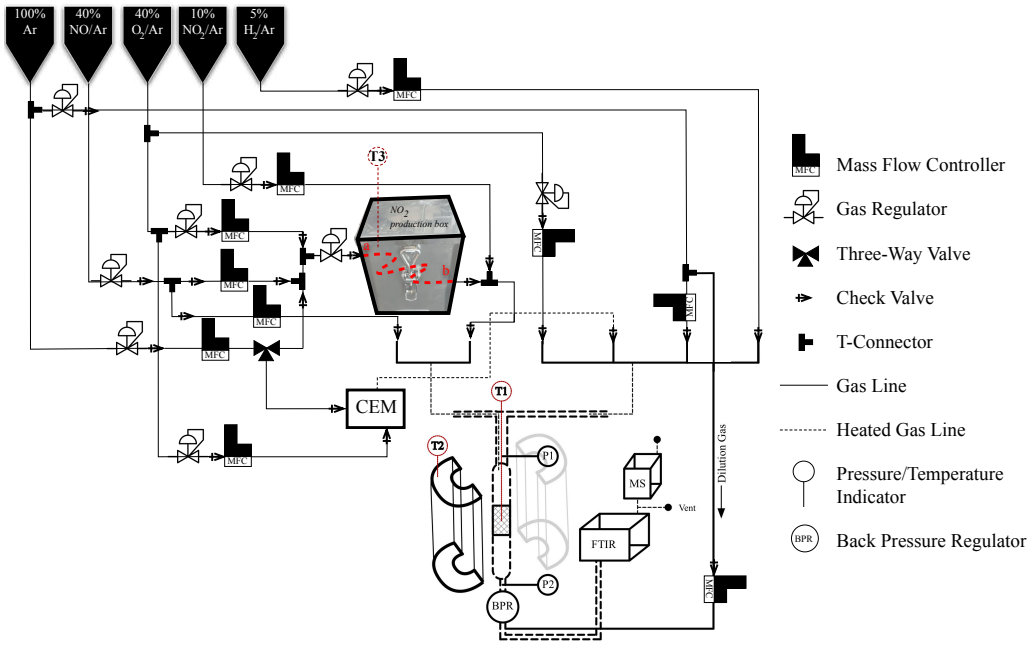

Figure 2. Experimental setup used of catalytic testing and *in-situ* production of NO_2. All (- - -) dashed lines are heated to 200°C to avoid cold spots and acid condensation. The dashed lines a-b (- - -) represent a coiled line section immersed in cooling water for *in-situ* conversion of NO to NO_2.

3. Results and Discussion

20 monometallic and 4 bimetallic catalysts were successfully prepared and tested for their capacity to oxidise NO in the presence and absence of NO_2 as a function of temperature (150-400°C). Table 2 presents catalyst surface areas, metal dispersion for the different catalysts, and apparent activation energies in the presence and absence of NO_2. The catalyst surface area decreased slightly with metal impregnation. The major drop in surface area was seen when bimetallic ruthenium-manganese catalysts were prepared with manganese loading larger than 10wt.%.

Preprints (www.preprints.org) | NOT PEER-REVIEWED | Posted: 10 October 2023 doi:10.20944/preprints202310.0537.v1

Table 2. BET surface areas (N_2 physisorption) and respective total metal dispersion (%) from chemisorption measurements for the different catalysts.

Catalyst	Surface[a] Area [m^2/g]	Dispersion [%][b]	Metal:Probe Specie	Probe Gas Uptake [mol g^{-1}]
CeO_2	92	–	–	–
Cr_{CeO_2}	78	–	–	–
Mn_{CeO_2}	82	–	–	–
Fe_{CeO_2}	82	3%	1:1 - Fe:H [29]	2
Co_{CeO_2}	80	10%	1:1 - Co:H [30,31]	27
Ni_{CeO_2}	79	11%	1:1 - Ni:H [32]	33
Y_{CeO_2}	85	–	–	–
Zr_{CeO_2}	86	–	–	–
Nb_{CeO_2}	79	–	–	–
Ru_{CeO_2}	72	41%	1:1 - Ru:CO [33,34]	39
Ru_{Mn_5,CeO_2}	71	39%	1:1 - Ru:CO [33,34]	35
Ru_{Mn_{10},CeO_2}	65	32%	1:1 - Ru:CO [33,34]	31
Ru_{Mn_{15},CeO_2}	55	19%	1:1 - Ru:CO [33,34]	18
Ru_{Mn_{20},CeO_2}	48	13%	1:1 - Ru:CO [33,34]	12
Rh_{CeO_2}	74	38%	1:1 - Rh:H [35]	39
Pd_{CeO_2}	72	–	–	–
Ag_{CeO_2}	70	29%	1:1 - Ag:H_2 [36]	24
Sn_{CeO_2}	80	–	–	–
Re_{CeO_2}	75	–	–	–
Ir_{CeO_2}	76	37%	1:1 - Ir:CO [37]	35
Pt_{CeO_2}	75	43%	1:1 - Pt:CO [21]	42
Au_{CeO_2}	72	2%	1:1 - Au:H [38]	2
Pb_{CeO_2}	70	–	–	–
Gd_{CeO_2}	81	–	–	–
Er_{CeO_2}	77	–	–	–

a. Average of two parallel experiments with the same material. b. Dispersion measurement programme details are presented in Table S1.

Table S1 details metal dispersion programme and Table 2 presents dispersion results. The dispersion analysis programme and probe specie were adjusted for different metal catalysts, and it was not possible to calculate dispersion for the Cr_{CeO_2}, Mn_{CeO_2}, Y_{CeO_2}, Zr_{CeO_2}, Nb_{CeO_2}, Pd_{CeO_2}, Sn_{CeO_2}, Re_{CeO_2}, Pb_{CeO_2}, Gd_{CeO_2} and Er_{CeO_2} catalysts. Among monometallic catalysts, the decreasing order of catalyst metal dispersion was $Pt_{CeO_2} > Rh_{CeO_2} > Ir_{CeO_2} > Ru_{CeO_2} > Ag_{CeO_2} > Fe_{CeO_2} \approx Co_{CeO_2} > Ni_{CeO_2} \approx Au_{CeO_2}$. The bimetallic catalyst dispersion analysis was also challenging due to the presence of Mn, however, CO chemisorption was performed on these bimetallic catalysts, assuming exclusive adsorption of CO on Ru. Similar to the surface area of bimetallic catalysts, the dispersion was also reduced with increased manganese loading.

Comparison plots for apparent activation energy for all monometallic and bimetallic catalysts are presented in Figures 3 and 4 respectively. The apparent activation energy calculations proved to be difficult for Sn_{CeO_2}, Gd_{CeO_2}, Er_{CeO_2} and Re_{CeO_2} in feed(i) and few of the monometallic catalysts have been omitted for apparent activation energy calculations due to low catalytic activity in the actual temperature range (presented in (d)-(f) of Figure S3). Figures S5 and S6 present the Arrhenius plot fit for all monometallic catalysts in feed (i) and (ii), respectively. Table S2 presents goodness-of-fit R^2 parameter for the Arrhenius plots and respective activation energies. From Figure 3 and Table S2, in feed(i) apparent activation energy of Period 4 metal-containing catalysts and Pt_{CeO_2} catalyst were the lowest with good Arrhenius plot fit. The bimetallic catalysts had reasonable activation energies when compared to monometallic Ru and Mn catalysts in feed (i) (see Figures 3 and 4). The activation energy for bimetallic RuMn first decreased to 39.4kJ/mol with 10wt.% manganese loading and then increased two-fold for the Ru_{Mn_{20},CeO_2} catalyst in feed (i) (see Figure 4 and Table S2).

Preprints (www.preprints.org) | NOT PEER-REVIEWED | Posted: 10 October 2023 doi:10.20944/preprints202310.0537.v1

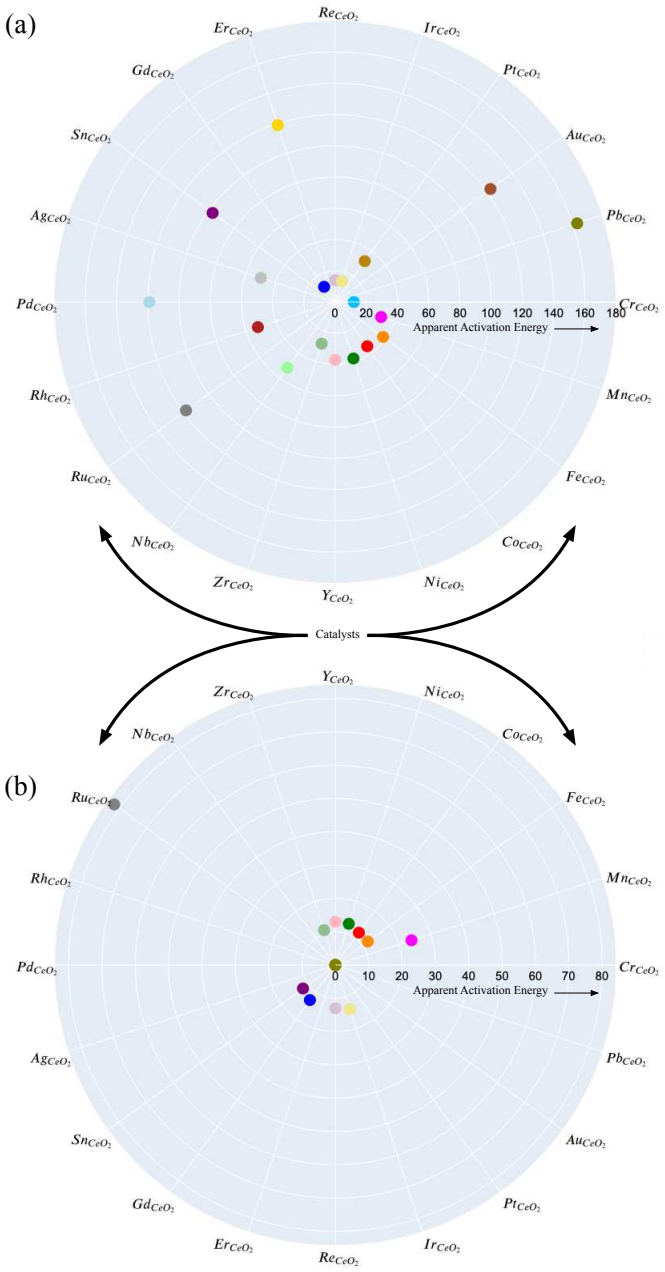

Figure 3. Apparent activation energy (E_a kJ/mol) in two different feeds; (a) Feed (i) 10% NO, 6% O_2, 15% H_2O and rest Ar and (b) Feed (ii) 8% NO, 2% NO_2 5% O_2, 15% H_2O and rest Ar, with a space velocity of 24,000 $Ncm^3/g_{gcat}h$ for different monometallic catalysts.

Preprints (www.preprints.org) | NOT PEER-REVIEWED | Posted: 10 October 2023 doi:10.20944/preprints202310.0537.v1

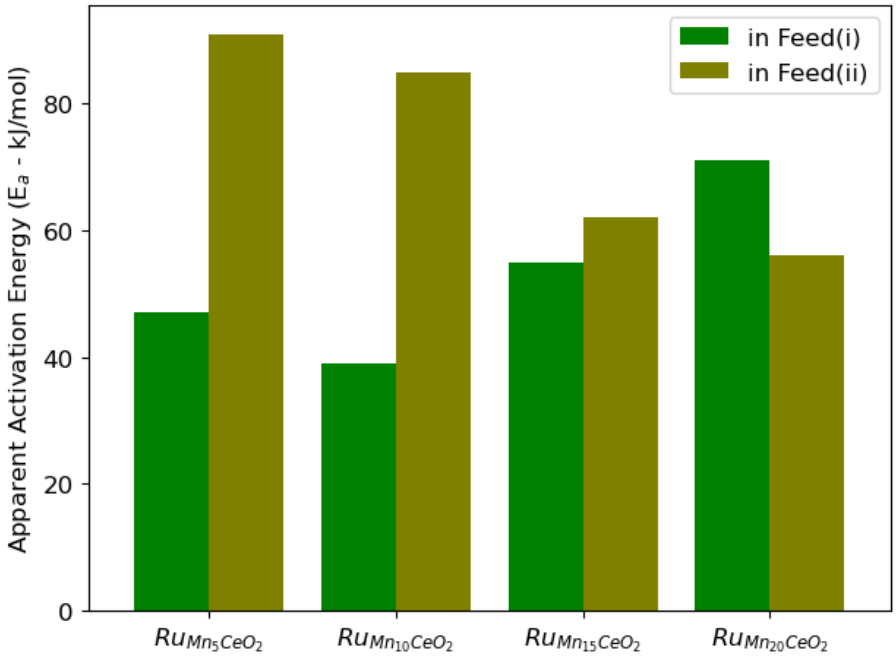

Figure 4. Apparent activation energy (E_a kJ/mol) in two different feeds; (a) Feed (i) 10% NO, 6% O_2, 15% H_2O and rest Ar and (b) Feed (ii) 8% NO, 2% NO_2 5% O_2, 15% H_2O and rest Ar, with a space velocity of 24,000 $Ncm^3/g_{gcat}h$ for different bimetallic catalysts.

Figure 5 presents X-ray diffractograms for all as-prepared bimetallic catalysts, Mn_{CeO_2} and Ru_{CeO_2} catalysts, diffractograms for all other monometallic catalysts are presented in Figure S4. From diffractograms of all monometallic catalysts (presented in Figure S4), the fluorite cubic structure of CeO_2 is maintained upon doping with different elements. Only Ru_{CeO_2} and Mn_{CeO_2} catalysts had other distinct diffraction peaks than from that of CeO_2, which corresponds to RuO_2 (presented as * in Figure S4) and MnO_2 (presented as △ in Figure S4) respectively, indicating larger RuO_2 particles for these catalysts. The bimetallic Ru-Mn catalysts (Ru_{Mn_5,CeO_2}, Ru_{Mn_{10},CeO_2}, Ru_{Mn_{15},CeO_2} and Ru_{Mn_{20},CeO_2}), had RuO_2 peaks in their respective diffractograms (presented in Figure 5). However, the presence of MnO_2 peaks was more evident when the Mn loading was 10wt.% and above. As for the monometallic catalysts, the fluorite structure of ceria was maintained also in the bimetallic catalysts.

Figures S3, S5 and S6 presents catalytic NO conversions with respect to temperature and activation energy (in the temperature range of 340-350°C) of different monometallic ceria-supported catalysts in feed (i) and (ii) grouped and presented by periods in the periodic table for comparison. Among the monometallic catalysts, Period 4 metal-containing catalysts were more active than the rest of the monometallic catalysts at temperatures below 320°C. Out of all monometallic catalysts, only Ru_{CeO_2} and Ir_{CeO_2} attained NO-NO_2 equilibrium in the measured temperature range for feed (i) and only Ru_{CeO_2} for feed (ii). The majority of monometallic catalysts had activity in feed (ii) similar to that of gas-phase conversion with only CeO_2, indicating NO_2 as an activity inhibitor as discussed by Mulla et al. [15] for platinum catalysts. Figure 6 presents average catalytic conversion at 380°C for all monometallic catalysts and the CeO_2 support in feed (i) and (ii) during temperature scan (150-400°C) at WHSV= 24,000 $Ncm^3/g_{gcat}h$ at ambient pressure. The addition of NO_2 in feed(ii) reduced the catalytic activity of all monometallic catalysts (presented in (d)-(f) Figures S3 and 6). Mn_{CeO_2}, Fe_{CeO_2}, Ru_{CeO_2} and Ir_{CeO_2} catalysts were the most promising monometallic catalysts in terms of catalytic activity in both feed compositions (i) and (ii).

Preprints (www.preprints.org) | NOT PEER-REVIEWED | Posted: 10 October 2023 doi:10.20944/preprints202310.0537.v1

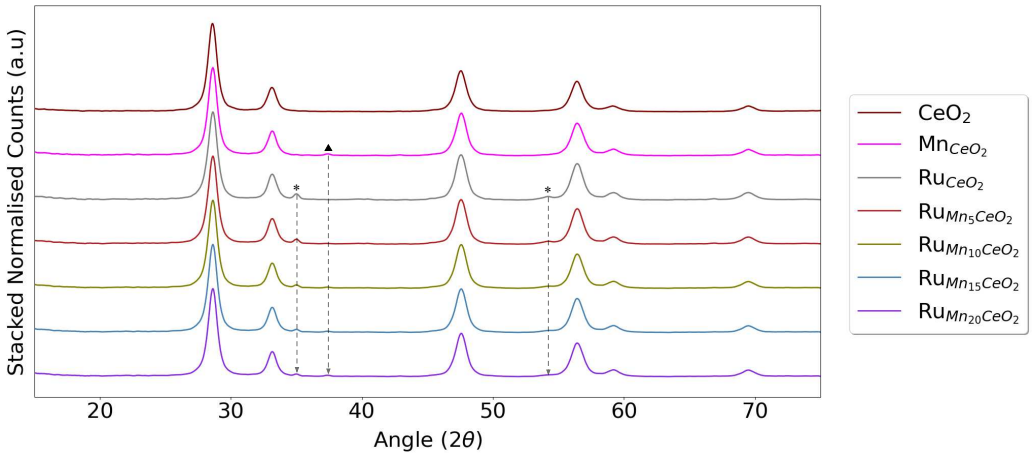

Figure 5. X-ray diffraction (XRD) patterns recorded for the CeO_2 support (PDF-00-034-0394), with Mn_{CeO_2}, Ru_{CeO_2}, Ru_{Mn_5,CeO_2}, Ru_{Mn_{10},CeO_2}, Ru_{Mn_{15},CeO_2} and Ru_{Mn_{20},CeO_2} catalyst samples in the 2θ range 5-75° with Cu K_α radiation (1.54060Å). Diffraction peaks of RuO_2 (PDF-04-003-2008) are represented as * and MnO_2 (PDF-04-007-3893) are presented as △

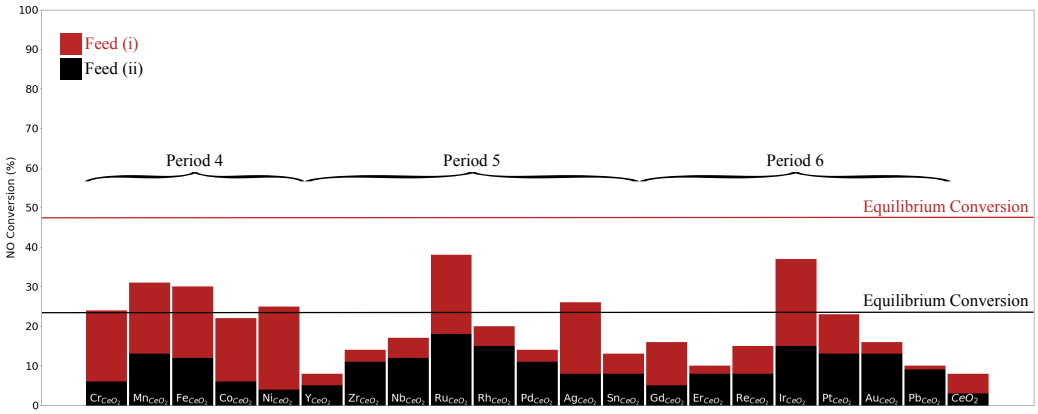

Figure 6. NO conversion (%) over various monometallic catalysts at 380°C during temperature scan (150-400°C) at WHSV= 24,000 $Ncm^3/g_{gcat}h$ at ambient pressure in Feed (i): 10% NO, 6% O_2, 15% H_2O and rest Ar and Feed (ii) 8% NO, 2% NO_2 5% O_2, 15% H_2O and rest Ar. Period 4 (from the Periodic table) metal catalysts are: Cr_{CeO_2}, Mn_{CeO_2}, Fe_{CeO_2}, Co_{CeO_2} and Ni_{CeO_2}, Period 5 metal catalysts are: Y_{CeO_2}, Zr_{CeO_2}, Nb_{CeO_2}, Ru_{CeO_2}, Rh_{CeO_2}, Pd_{CeO_2}, Ag_{CeO_2} and Sn_{CeO_2}, and Period 6 metal catalysts are Gd_{CeO_2}, Er_{CeO_2}, Re_{CeO_2}, Ir_{CeO_2}, Pt_{CeO_2}, Au_{CeO_2} and Pb_{CeO_2}. NO conversion (%) at 380°C presented above for all catalysts are average conversions of three parallel temperature scans (150-400°C) in feed (i) and (ii).

Catalyst selection rules dictate for active, cost-effective, versatile, selective, and stable catalysts [39,40]. Ru_{CeO_2} and Ir_{CeO_2} are the most active catalysts, but lower cost efficiency in comparison with Mn_{CeO_2} and Fe_{CeO_2} catalysts [27]. Ruthenium is more known for its versatility in catalysis compared to iridium due to its lower ionisation energy and more accessible range of oxidation states (-2 to +8)[41]. Manganese-based catalysts are used for low-temperature NO oxidation reactions at lower concentrations of NO [42–44] and our previous research portrayed that the 72hr isothermal activity of manganese on zirconia catalysts for NO oxidation at industrial nitric acid conditions can be improved by doping with Ag [20]. The highest achievable oxidation state in the first row of d-block elements increases up to manganese and decreases towards zinc. Manganese has multiple stable oxidation states (+2 to +7) and thus higher redox potential than the neighbouring element iron [45].

From the above literature and results presented in Figures S3 and 6 and Table 2, manganese-based catalysts can participate in oxygen activation and transfer processes, whereas the presence of ruthenium can contribute to catalytic activity and stability [42–44,46,47]. A combination of Ru-Mn bimetallic catalysts suggests a pathway for producing catalysts for NO to NO_2 oxidation with significant

Preprints (www.preprints.org) | NOT PEER-REVIEWED | Posted: 10 October 2023 doi:10.20944/preprints202310.0537.v1

low-temperature activity and lower activation energy. The Ru_{Mn_5,CeO_2}, Ru_{Mn_{10},CeO_2}, Ru_{Mn_{15},CeO_2} and Ru_{Mn_{20},CeO_2} catalysts are four Ru-Mn bimetallic catalysts on ceria support with increasing loading of manganese.

Figures 7 and 8 presents NO to NO_2 conversion for Mn_{CeO_2}, Ru_{CeO_2}, Ru_{Mn_5,CeO_2}, Ru_{Mn_{10},CeO_2}, Ru_{Mn_{15},CeO_2} and Ru_{Mn_{20},CeO_2} catalysts in feed (i) and (ii). Similar to conversions of monometallic catalysts, the NO conversion of bimetallic catalysts were severely inhibited by the presence of NO_2 in the feed due to competitive adsorption of NO_2 on the catalyst surface. The addition of 5wt.% manganese to the Ru_{CeO_2} catalyst improved low-temperature catalytic activity in feed(i), whereas catalytic activity in feed (ii) remained similar to that of the Ru_{CeO_2} catalyst. Increasing manganese loading higher than 10wt.% resulted in a decrease in catalytic activity for Ru_{Mn_{15},CeO_2} and Ru_{Mn_{20},CeO_2} catalysts in both feed (i) and (ii). The apparent activation energy in feed (i) and (ii) for the bimetallic catalysts are presented in Table 2 and respective Arrhenius plots are presented in Figures S7 and S8. The Ru_{Mn_{10},CeO_2} catalyst proved to be the most active catalyst with an apparent activation energy of 39.4 kJ/mol and 85.4 kJ/mol in feed (i) and (ii) respectively.

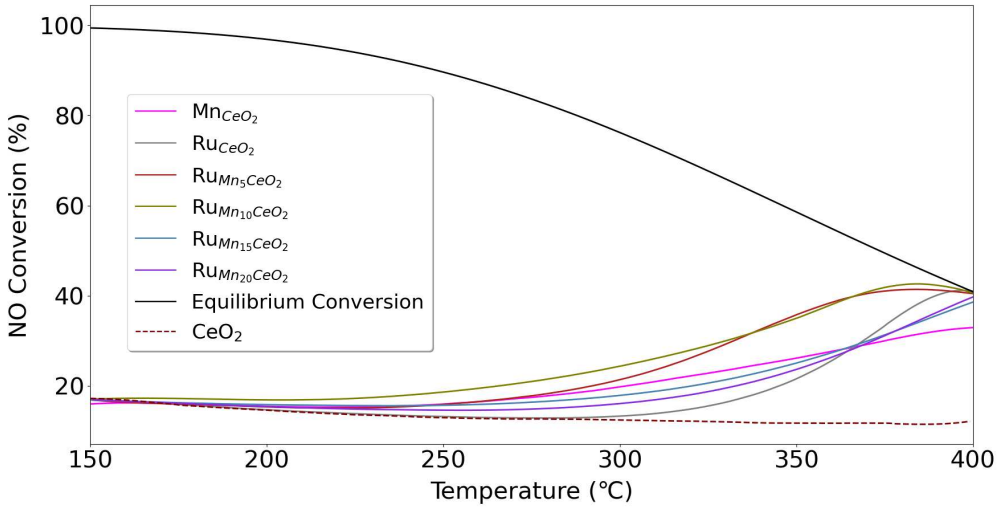

Figure 7. NO conversion (%) of Mn_{CeO_2}, Ru_{CeO_2}, Ru_{Mn_5,CeO_2}, Ru_{Mn_{10},CeO_2}, Ru_{Mn_{15},CeO_2} and Ru_{Mn_{20},CeO_2} catalysts as a function of temperature with Feed (i): 10% NO, 6% O_2, 15% H_2O and rest Ar, heated at a rate of 5°C/min at WHSV= 24,000 $Ncm^3/g_{gcat}h$ at ambient pressure.

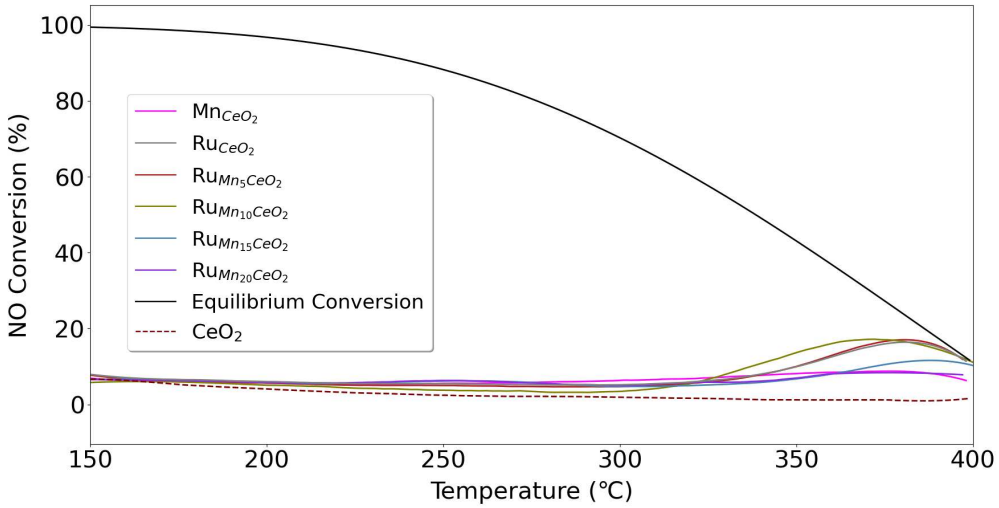

Figure 8. NO conversion (%) of Mn_{CeO_2}, Ru_{CeO_2}, Ru_{Mn_5,CeO_2}, Ru_{Mn_{10},CeO_2}, Ru_{Mn_{15},CeO_2} and Ru_{Mn_{20},CeO_2} catalysts as a function of temperature with Feed (ii): 8% NO, 2% NO_2, 5% O_2, 15% H_2O and rest Ar, heated at a rate of 5°C/min at WHSV= 24,000 $Ncm^3/g_{gcat}h$ at ambient pressure.

Preprints (www.preprints.org) | NOT PEER-REVIEWED | Posted: 10 October 2023 doi:10.20944/preprints202310.0537.v1

Figure 9 presents 45hrs isothermal runs for Mn_{CeO_2}, Ru_{CeO_2}, Ru_{Mn_{10},CeO_2} and the CeO_2 support at 320°C in 10% NO, 6% O_2, 15% H_2O and rest Ar at WHSV= 24,000 $Ncm^3/g_{gcat}h$ at ambient pressure. The isothermal activity of the Ru_{CeO_2} and Ru_{Mn_{10},CeO_2} catalyst stabilised after 10hrs of the experimental run. However, NO conversion for Mn_{CeO_2} decreased over time and eventually resembling the NO conversion obtained over the CeO_2 support, thus indicating deactivation. This deactivation of manganese can be due to MnO_2 reducing to Mn_2O_3 as previously seen for Mn/ZrO_2 catalysts [20]. The addition of 10wt.% manganese clearly enhanced the low-temperature activity of the Ru_{CeO_2} catalyst and the catalyst was stable throughout 45hrs of an isothermal run at 320°C at ambient pressure.

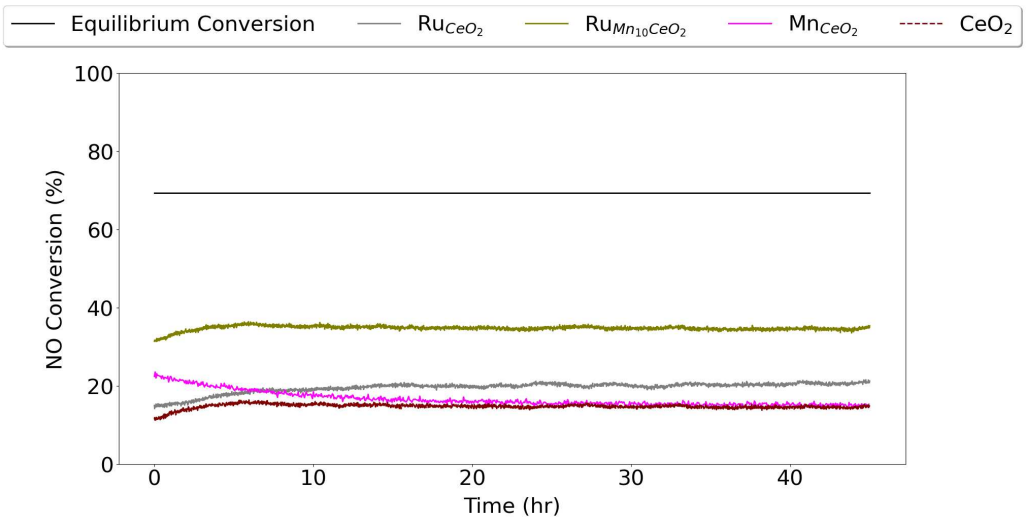

Figure 9. NO conversion (%) of Mn_{CeO_2}, Ru_{CeO_2}, Ru_{Mn_{10},CeO_2} and the CeO_2 support at 320°C in 10% NO, 6% O_2, 15% H_2O and rest Ar at WHSV= 24,000 $Ncm^3/g_{gcat}h$ at ambient pressure for 45hrs.

4. Conclusions

This work has explored various monometallic and bimetallic catalysts for NO to NO_2 oxidation at industrial nitric acid production conditions. The effect of temperature was investigated, along with the inhibition effect of the product NO_2 in the feed. Among all monometallic catalysts, Period 4 metal-containing catalysts had the highest low-temperature NO oxidation activity. However, the Ru_{CeO_2} and Ir_{CeO_2} catalysts were the only two catalysts that could reach NO-NO_2 equilibrium in the measured temperature range (150-400°C) in the absence of NO_2 in the feed. In the presence of NO_2, only the Ru_{CeO_2} catalyst reached equilibrium conversion at 400°C with an apparent activation energy of 81.7 kJ/mol. In comparison to most monometallic catalysts, bimetallic catalysts with 5 and 10wt.% manganese loading attained NO-NO_2 equilibrium in presence and absence of NO_2 at lower temperatures (ca. 400°C). The Ru_{Mn_{10},CeO_2} catalyst proved to be the most active catalyst with an apparent activation energy of 39.4 kJ/mol and 85.4 kJ/mol in the absence and presence of NO_2, respectively. These results illustrate that the CeO_2-supported bimetallic ruthenium-manganese catalysts are promising for oxidising NO to NO_2 at low temperatures in industrial nitric acid production conditions.

Author Contributions: **Jithin Gopakumar:** Conceptualization, Methodology, Validation, Formal analysis, Investigation, Writing – Original Draft, Writing – Review & Editing, Visualization **Albert Miro i Rovira:** Investigation, Formal analysis, Validation **Bjørn Christian Enger:** Conceptualization, Validation, Writing – Review & Editing, Supervision, Funding acquisition **David Waller:** Conceptualization, Validation, Writing – Review & Editing, Supervision, Funding acquisition **Magnus Rønning:** Conceptualization, Validation, Writing – Review & Editing, Supervision, Project Administration, Funding acquisition.

Funding: This project is funded by iCSI (industrial Catalysis Science and Innovation) Centre for research-based innovation from the Research Council of Norway (grant 237922).

Data Availability Statement: Research data will be made available upon request.

Acknowledgments: This work was carried out at Norges teknisk-naturvitenskapelige universitet (NTNU) and is gratefully acknowledged for its support.

Conflicts of Interest: The authors declare no competing interest.

Abbreviations

The following abbreviations are used in this manuscript:

CAPEX	Capital Expenditure
PGM	Platinum Group Metals
WHSV	Weight Hourly Space Velocity

References

1. Honti, G.D. *The Nitrogen Industry*, 1976 ed.; Vol. 48, Akadémiai Kiadó, 1976. doi:10.1002/cite.330481234.
2. Travis, A.S. *Nitrogen Capture*; Springer International Publishing: Cham, 2018. doi:10.1007/978-3-319-68963-0.
3. Moulijn, J.A. Chemical process technology. *Choice Reviews Online* **2013**, *51*, 51–2107. doi:10.5860/CHOICE.51-2107.
4. Grande, C.A.; Andreassen, K.A.; Cavka, J.H.; Waller, D.; Lorentsen, O.A.; Øien, H.; Zander, H.J.; Poulston, S.; García, S.; Modeshia, D. Process Intensification in Nitric Acid Plants by Catalytic Oxidation of Nitric Oxide. *Industrial and Engineering Chemistry Research* **2018**, *57*, 10180–10186. doi:10.1021/acs.iecr.8b01483.
5. YAO, H. Ceria in automotive exhaust catalysts I. Oxygen storage. *Journal of Catalysis* **1984**, *86*, 254–265. doi:10.1016/0021-9517(84)90371-3.
6. Su, E.; Montreuil, C.; Rothschild, W. Oxygen storage capacity of monolith three-way catalysts. *Applied Catalysis* **1985**, *17*, 75–86. doi:10.1016/S0166-9834(00)82704-9.
7. Courtois, X.; Bion, N.; Marécot, P.; Duprez, D. Chapter 8 The role of cerium-based oxides used as oxygen storage materials in DeNOx catalysis; 2007; pp. 235–259. doi:10.1016/S0167-2991(07)80209-6.
8. Montini, T.; Melchionna, M.; Monai, M.; Fornasiero, P. Fundamentals and Catalytic Applications of CeO 2 -Based Materials. *Chemical Reviews* **2016**, *116*, 5987–6041. doi:10.1021/acs.chemrev.5b00603.
9. Inger, M.; Rajewski, J.; Ruszak, M.; Wilk, M. The influence of NOx presence on the catalytic N2O decomposition over the supported double-promoted cobalt spinel catalyst. *Chemical Papers* **2019**, *73*, 1979–1986. doi:10.1007/s11696-019-00750-9.
10. Yung, M.M.; Holmgreen, E.M.; Ozkan, U.S. Cobalt-based catalysts supported on titania and zirconia for the oxidation of nitric oxide to nitrogen dioxide. *Journal of Catalysis* **2007**, *247*, 356–367. doi:10.1016/j.jcat.2007.02.020.
11. Chen, H.; Wang, Y.; Lv, Y.K. Catalytic oxidation of NO over MnO2 with different crystal structures. *RSC Advances* **2016**, *6*, 54032–54040. doi:10.1039/c6ra10103h.
12. Salman, A.U.R.; Hyrve, S.M.; Regli, S.K.; Zubair, M.; Enger, B.C.; Lødeng, R.; Waller, D.; Rønning, M. Catalytic Oxidation of NO over LaCo1-xBxO3 (B = Mn, Ni) Perovskites for Nitric Acid Production. *Catalysts* **2019**, *9*, 429. doi:10.3390/catal9050429.
13. Chen, J.; Shen, M.; Wang, X.; Qi, G.; Wang, J.; Li, W. The influence of nonstoichiometry on LaMnO3 perovskite for catalytic NO oxidation. *Applied Catalysis B: Environmental* **2013**, *134-135*, 251–257. doi:10.1016/j.apcatb.2013.01.027.
14. Olsson, L.; Persson, H.; Fridell, E.; Skoglundh, M.; Andersson, B. A Kinetic Study of NO Oxidation and NO x Storage on Pt/Al2O3 and Pt/BaO/Al2O3 *The Journal of Physical Chemistry B* **2001**, *105*, 6895–6906.
15. Mulla, S.S.; Chen, N.; Delgass, W.N.; Epling, W.S.; Ribeiro, F.H. NO 2 inhibits the catalytic reaction of NO and O 2 over Pt. *Catalysis Letters* **2005**, *100*, 267–270. doi:10.1007/s10562-004-3466-1.
16. Smeltz, A.; Getman, R.; Schneider, W.; Ribeiro, F. Coupled theoretical and experimental analysis of surface coverage effects in Pt-catalyzed NO and O2 reaction to NO2 on Pt(111). *Catalysis Today* **2008**, *136*, 84–92. doi:10.1016/j.cattod.2007.12.139.
17. Xue, E.; Seshan, K.; Ross, J.R.H. Roles of supports , Pt loading and Pt dispersion in the oxidation of NO to NO , and of SO , to SO ,. *Applied Catalysis B: Environmental* **1996**, *11*, 65–79.

18. Hong, Z.; Wang, Z.; Li, X. Catalytic oxidation of nitric oxide (NO) over different catalysts: an overview. *Catalysis Science & Technology* **2017**, *7*, 3440–3452. doi:10.1039/C7CY00760D.
19. Gopakumar, J.; Benum, P.M.; Svenum, I.H.; Enger, B.C.; Waller, D.; Rønning, M. Redox transformations of Ru catalyst during NO oxidation at industrial nitric acid production conditions. *Chemical Engineering Journal* **2023**, p. 146406. doi:10.1016/j.cej.2023.146406.
20. Gopakumar, J.; Vold, S.; Enger, B.C.; Waller, D.; Vullum, P.E.; Rønning, M. Catalytic oxidation of NO to NO 2 for industrial nitric acid production using Ag-promoted MnO2/ZrO2 catalysts. *Catalysis Science & Technology* **2023**, *13*, 2783–2793. doi:10.1039/D2CY02178A.
21. Salman, A.u.R.; Enger, B.C.; Auvray, X.; Lødeng, R.; Menon, M.; Waller, D.; Rønning, M. Catalytic oxidation of NO to NO2 for nitric acid production over a Pt/Al2O3 catalyst. *Applied Catalysis A: General* **2018**, *564*, 142–146. doi:10.1016/j.apcata.2018.07.019.
22. William C. Klingelhoefer, S. Nitric Oxide Oxidation, 1938.
23. Heilig, M.L. Process of Oxidizing Gases, 1994. doi:10.1145/178951.178972.
24. Andersen, H.C.; Haley, A.J. Process for the oxidation of nitric oxide, 1963.
25. Robertus J. M. Klein Gebbink.; Marc-Etienne Moret. *Non-Noble Metal Catalysis*; Wiley-VCH Verlag GmbH & Co. KGaA: Weinheim, Germany, 2019. doi:10.1002/9783527699087.
26. Védrine, J.C. Metal Oxides in Heterogeneous Oxidation Catalysis: State of the Art and Challenges for a More Sustainable World. *ChemSusChem* **2019**, *12*, 577–588. doi:10.1002/cssc.201802248.
27. European Commission. Critical Raw Materials Factsheets (2020). Technical report, 2020. doi:10.2873/92480.
28. Fogler, H.S. *Elements of Chemical Reaction Engineering*; 2006.
29. Mosallanejad, S.; Dlugogorski, B.Z.; Kennedy, E.M.; Stockenhuber, M. On the Chemistry of Iron Oxide Supported on γ-Alumina and Silica Catalysts. *ACS Omega* **2018**, *3*, 5362–5374. doi:10.1021/acsomega.8b00201.
30. Taher, N.M.; Mahmoudi, M.; Sajjadivand, S.S. Cobalt Catalysts Preparation and Characterization over Alumina Support for Fischer Tropsch Synthesis. *Biofuels Engineering* **2017**, *2*, 51–61. doi:10.1515/bfuel-2017-0004.
31. Robert C. Reuel.; Calvin H. Bartholomew. The stoichiometries of H2 and CO adsorptions on cobalt: Effects of support and preparation. *Journal of Catalysis* **1984**, *85*, 63–77. doi:10.1016/0021-9517(84)90110-6.
32. Niu, J.; Liland, S.E.; Yang, J.; Rout, K.R.; Ran, J.; Chen, D. Effect of oxide additives on the hydrotalcite derived Ni catalysts for CO2 reforming of methane. *Chemical Engineering Journal* **2019**, *377*, 119763. doi:10.1016/j.cej.2018.08.149.
33. Kim, H.B.; Park, E.D. Ammonia decomposition over Ru catalysts supported on alumina with different crystalline phases. *Catalysis Today* **2023**, *411-412*, 113817. doi:10.1016/j.cattod.2022.06.032.
34. Zhang, Y.; Yang, X.; Yang, X.; Duan, H.; Qi, H.; Su, Y.; Liang, B.; Tao, H.; Liu, B.; Chen, D.; Su, X.; Huang, Y.; Zhang, T. Tuning reactivity of Fischer–Tropsch synthesis by regulating TiOx overlayer over Ru/TiO2 nanocatalysts. *Nature Communications* **2020**, *11*, 3185. doi:10.1038/s41467-020-17044-4.
35. Choong, C.K.S.; Chen, L.; Du, Y.; Schreyer, M.; Daniel Ong, S.W.; Poh, C.K.; Hong, L.; Borgna, A. The role of metal–support interaction for CO-free hydrogen from low temperature ethanol steam reforming on Rh–Fe catalysts. *Physical Chemistry Chemical Physics* **2017**, *19*, 4199–4207. doi:10.1039/C6CP05934A.
36. Guerra-Que, Z.; Torres-Torres, G.; Pérez-Vidal, H.; Cuauhtémoc-López, I.; Espinosa de los Monteros, A.; Beltramini, J.N.; Frías-Márquez, D.M. Silver nanoparticles supported on zirconia–ceria for the catalytic wet air oxidation of methyl tert-butyl ether. *RSC Advances* **2017**, *7*, 3599–3610. doi:10.1039/C6RA25684H.
37. MCVICKER, G. Chemisorption properties of iridium on alumina catalysts. *Journal of Catalysis* **1980**, *65*, 207–220. doi:10.1016/0021-9517(80)90295-X.
38. Bus, E.; Miller, J.T.; van Bokhoven, J.A. Hydrogen Chemisorption on Al2O3-Supported Gold Catalysts. *The Journal of Physical Chemistry B* **2005**, *109*, 14581–14587. doi:10.1021/jp051660z.
39. Kühn, F.E. Catalysis. From Principles to Applications. By Matthias Beller, Albert Renken and Rutger A. van Santen. *Angewandte Chemie International Edition* **2013**, *52*, 2650–2650. doi:10.1002/anie.201210089.
40. Larsen, G. Principles and Practice of Heterogeneous Catalysis By J. M. Thomas (University of Cambridge) and W. J. Thomas (University of Bath). VCH: Weinheim, 1997. xxiii + 669 pp. DM88.00. ISBN 3-527-29239-X. *Journal of the American Chemical Society* **1997**, *119*, 11560–11560. doi:10.1021/ja975538s.
41. Bruneau, C.; Dixneuf, P.H. *Ruthenium in catalysis*; Vol. 48, 2014. doi:10.1007/978-3-319-08482-4.

42. LI, H.; TANG, X.; YI, H.; YU, L. Low-temperature catalytic oxidation of NO over Mn-Ce-Ox catalyst. *Journal of Rare Earths* **2010**, *28*, 64–68. doi:10.1016/S1002-0721(09)60052-1.
43. Li, K.; Tang, X.; Yi, H.; Ning, P.; Kang, D.; Wang, C. Low-temperature catalytic oxidation of NO over Mn-Co-Ce-Ox catalyst. *Chemical Engineering Journal* **2012**, *192*, 99–104. doi:10.1016/j.cej.2012.03.087.
44. Chen, H.; Wang, Y.; Lyu, Y.K. High catalytic activity of Mn-based catalyst in NO oxidation at low temperature and over a wide temperature span. *Molecular Catalysis* **2018**, *454*, 21–29. doi:10.1016/j.mcat.2018.05.001.
45. Johnstone, A.H. CRC Handbook of Chemistry and Physics-69th Edition Editor in Chief R. C. Weast, CRC Press Inc., Boca Raton, Florida, 1988, pp. 2400, price £57.50. ISBN 0-8493-0369-5. *Journal of Chemical Technology & Biotechnology* **2007**, *50*, 294–295. doi:10.1002/jctb.280500215.
46. Takashima, T.; Hashimoto, K.; Nakamura, R. Mechanisms of pH-dependent activity for water oxidation to molecular oxygen by MnO2 electrocatalysts. *Journal of the American Chemical Society* **2012**, *134*, 1519–1527. doi:10.1021/ja206511w.
47. Cao, L.; Luo, Q.; Chen, J.; Wang, L.; Lin, Y.; Wang, H.; Liu, X.; Shen, X.; Zhang, W.; Liu, W.; Qi, Z.; Jiang, Z.; Yang, J.; Yao, T. Dynamic oxygen adsorption on single-atomic Ruthenium catalyst with high performance for acidic oxygen evolution reaction. *Nature Communications* **2019**, *10*. doi:10.1038/s41467-019-12886-z.